Modeling water mass formation in the Mertz Glacier Polynya and Adélie Depression, East Antarctica

S. J. Marsland[1,2]

Division of Marine Research, Commonwealth Scientific and Industrial Research Organisation, Hobart, Australia

N. L. Bindoff,[3,4] G. D. Williams,[4] and W. F. Budd[4]

Antarctic Climate and Ecosystems Cooperative Research Centre, Hobart, Australia

Received 18 April 2004; revised 11 July 2004; accepted 4 August 2004; published 4 November 2004.

[1] High rates of sea ice growth and brine rejection in the Mertz Glacier Polynya drive the production of dense continental shelf waters in the Adélie Depression. We consider the rate of outflow of waters having sufficient density to sink into the neighboring abyssal ocean and form Adélie Land Bottom Water (ALBW). Along with Weddell and Ross Sea Bottom Waters, the ALBW is an important source of Antarctic Bottom Water. The relevant processes are modeled using a variant of the Max Planck Institute Ocean Model (MPIOM) under daily NCEP-NCAR reanalysis forcing for the period 1991–2000. The orthogonal curvilinear horizontal grid allows for the construction of a global domain with high resolution in our region of interest. The modeled Mertz Glacier Polynya is realistic in location and extent, exhibiting low ice thickness (<0.4 m) and low ice fraction (<50%). The net surface ocean to atmosphere heat flux exceeds 200 W m^2 and is dominated by sensible heat exchange. In wintertime (May through September inclusive), 7.5 m of sea ice forms over the Adélie Depression at a rate of 4.9 cm d^{-1}: this results in annual average volumetric production of 99 km^3 of sea ice. The associated brine release drives dense shelf water formation. The off-shelf flow of dense water exhibits strong interannual variability in response to variability in both atmospheric forcing and ocean preconditioning. Averaged over the period 1991–2000 the off shelf flow of dense water is 0.15 Sv: for a period of strong outflow (1993–1997), this increases to 0.24 Sv. Most of the outflow occurs during July through October, at a rate of 0.40 (0.63) Sv over the period 1991–2000 (1993–1997). The peak mean monthly outflow can exceed 1 Sv. *INDEX TERMS:* 4207 Oceanography: General: Arctic and Antarctic oceanography; 4255 Oceanography: General: Numerical modeling; 4283 Oceanography: General: Water masses; *KEYWORDS:* Southern Ocean, polynyas, modeling

Citation: Marsland, S. J., N. L. Bindoff, G. D. Williams, and W. F. Budd (2004), Modeling water mass formation in the Mertz Glacier Polynya and Adélie Depression, East Antarctica, *J. Geophys. Res.*, *109*, C11003, doi:10.1029/2004JC002441.

1. Introduction

[2] Antarctic Bottom Water (AABW) is the densest water mass in the global ocean [*Brennecke*, 1913a, 1913b; *Mosby*, 1934; *Orsi et al.*, 1999] and therefore of significance to our understanding of the Earth's climate. For example, it is of particular relevance to the lower limb of the global meridional overturning circulation [*Stommel*, 1958; *Stommel and Arons*, 1960a, 1960b] and the poleward transport of heat [*Orsi et al.*, 2002]. The traditional view has been that the primary source of AABW is Weddell Sea Bottom Water (WSBW) and the secondary source is Ross Sea Bottom Water (RSBW) [*Carmack*, 1977]. A third source, known as Adélie Land Bottom Water (ALBW), has been identified along the East Antarctic coastline in the Australia/New Zealand sector [*Gordon and Tchernia*, 1972; *Rodman and Gordon*, 1982]. Another source has also been identified in Prydz Bay, in the Indian sector of the Southern Ocean [*Schodlok et al.*, 2001]. The ALBW was believed to be only a very minor source: For example, in a bivariate (temperature and salinity) volumetric analysis of waters south of the Polar Front, *Carmack* [1977] estimated that ALBW constituted less than 0.5% of the total AABW. It was believed that the bottom waters found in the East Antarctic region were a mixture of WSBW flowing in from the west and RSBW flowing in from the east. However, the *Rintoul* [1998] analysis of hydrographic observations taken in the region as part of the World Ocean Circulation Experiment shows an oxygen maximum and silicate minimum much more indicative of locally sourced bottom waters. This led to a

[1] Formerly at Max-Planck-Institut für Meteorologie, Hamburg, Germany.

[2] Also at Antarctic Climate and Ecosystems Cooperative Research Centre, Hobart, Australia.

[3] Also at Division of Marine Research, Commonwealth Scientific and Industrial Research Organisation, Hobart, Australia.

[4] Also at Institute for Antarctic and Southern Ocean Studies, University of Tasmania, Hobart, Australia.

0148-0227/04/2004JC002441$09.00

reinterpretation of the volumetric potential temperature and salinity census of *Worthington* [1981]. Consequently, *Rintoul* [1998] suggests that the ALBW may be a more significant source of AABW than previously thought, accounting for as much as 25% of the total volume of AABW in the global ocean.

[3] The WSBW and RSBW is formed along wide continental shelves bounded by land to the west. This geometry allows the westward flowing shelf waters to reside on-shelf long enough that the density, which increases in time due to brine rejection associated with sea ice formation, becomes sufficient for bottom water formation [*Gill*, 1973]. In contrast, the ALBW is believed to have its source in one or more of the multitude of coastal polynyas that form in response to a strong and persistent katabatic wind regime [*Zwally et al.*, 1985; *Comiso and Gordon*, 1998; *Wendler et al.*, 1997]. A number of studies have suggested that the Mertz Glacier Polynya (MGP) and Adélie Depression are a likely source of ALBW. We have known since the work of *Gordon and Tchernia* [1972] that waters of sufficiently high density to form bottom water are present in the Adélie Depression. *Rintoul* [1998] reports a zonal transition in the hydrography of the off-shelf bottom waters around 143°E, corresponding with the deepest outlet of the Adélie Depression. Just east of the Adélie Depression outlet, *Fukamachi et al.* [2000] find that bottom water on the continental slope (140°E, 1317 m) is high in dissolved oxygen and low in silicate concentration relative to the waters above. They suggest this indicates that the downslope flow of dense water does not have a local source, but is more likely produced in the Adélie Depression immediately upstream. They also hypothesize that dense water from the Adélie Depression is the source of the seasonal signal in bottom temperature and current speed that they find in mooring data (139°E, 65°S, 2632 m). *Bindoff et al.* [2000] consider north-south hydrographic sections taken across the continental slope between 80°E and 150°E, and find that bottom tracer distribution is consistent with a source in the region 140°E–150°E, with warmer and fresher bottom waters to the west.

[4] Using satellite passive-microwave data, *Massom et al.* [1998] identified 28 coastal polynyas along the East Antarctic coastline (40°E–160°E). Using a 75% concentration criterion, they found the MGP to average 23,300 km^2, second in size only to the Shackleton Ice Shelf polynya (31,642 km^2). *Massom et al.* [1998] also noted the relative persistence, both in wintertime duration and interannual reoccurrence, of the MGP. Three factors combined may contribute to the MGP being a significant contributor to ALBW formation. First, the Mertz Glacier floating ice tongue and associated grounded iceberg extension (hereafter MGT) provide a barrier to the westward advection of sea ice associated with the Antarctic coastal current. Second, strong katabatic winds are suitably directed to force a wind-driven coastal polynya in the lee of the glacial ice barrier. Third, an on-shelf bathymetric depression allows for the local accumulation of dense waters that can spill out of the depression and if dense enough can form bottom water. For consistency with *Gordon and Tchernia* [1972] and *Rintoul* [1998], we call this bathymetric feature the Adélie Depression: It is also referred to as the George V Basin [*Porter-Smith*, 2003; *Beaman and Harris*, 2003].

[5] The above studies have all relied on hydrographic station data obtained during the summer season. Our knowledge of physical processes within the MGP is greatly enhanced by the July–August 1999 joint oceanographic [*Bindoff et al.*, 2001] and sea ice [*Lytle et al.*, 2001] observing program conducted aboard the RSV *Aurora Australis*. Hydrographic station data was collected over a loop repeated 3 times comprising a total of 87 CTD casts, and used by *Bindoff et al.* [2001] to identify four distinct water masses within the Adélie Depression. From the north a warm, fresh, and oxygen-depleted Highly Modified Circumpolar Deep Water (HMCDW) intrudes onto the shelf and flows eastward toward the MGT.

[6] The HMCDW interacts with a mode of relatively homogenous and therefore weakly stratified Low Salinity Shelf Water (LSSW). The LSSW was called Winter Water by *Williams and Bindoff* [2003]. Beneath the LSSW lies a relatively dense, more strongly stratified High Salinity Shelf Water (HSSW) within the Adélie Depression. To the south, they found a coastal return flow of super-cooled Ice Shelf Water (ISW) sourced from the MGT. Both the LSSW and the HSSW are of sufficient density to reach the bottom if adiabatically displaced into the neighboring abyssal plains of the Australian-Antarctic Basin. Potential temperature-salinity and oxygen-salinity scatter diagrams show a basically linear relationship, with LSSW lying between HMCDW (warm, fresh, low oxygen) and HSSW (cold, salty, rich in oxygen). *Bindoff et al.* [2001] use a simple water mass exchange model to conclude a sea ice growth rate of 4.9–7.7 cm d^{-1} averaged over the polynya area. Similar growth rates were estimated by *Williams and Bindoff* [2003] using a more sophisticated analysis based on the divergence of salt (fresh water) in the polynya region. This compares with a directly observed sea ice growth rate of 8 cm d^{-1}, with equal contributions from both thermodynamic and dynamic processes [*Lytle et al.*, 2001].

[7] Given the temporal and spatial sparsity of observations, General Circulation Models (GCMs) can further our understanding of the Mertz Polynya system and its role in water mass formation. To date, this has only been attempted with relatively coarse horizontal resolution GCMs. *Stössel and Markus* [2004] have assimilated satellite-observed coastal sea ice concentrations into their ocean and sea ice GCM, but the model resolution (3.5° in latitude and longitude) was insufficient to capture the MGP itself. *Wu et al.* [2003] do include the MGP in their assessment of the impact of Antarctic polynyas on the larger-scale circulation, but only in an atmosphere and sea ice GCM. The ocean and sea ice model used in the present study features a bipolar orthogonal curvilinear grid which allows for arbitrary placement and sizing of the model's poles. This allows for global grids with regionally high resolution. The main advantage is the avoidance of the nontrivial complications associated with the implementation of either open or closed boundary conditions. The resulting spatial discretization gives high horizontal resolution in the region of the MGP and Adélie Depression. We note that our region of interest is also a region where the incremental change between adjacent grid cell sizes (ddx = (dx1 − dx2)/(dx1 + dx2)) is at a minimum, and is far from the maxima which are preferred locations for partial reflections and potentially the areas of lowest accuracy in the model.

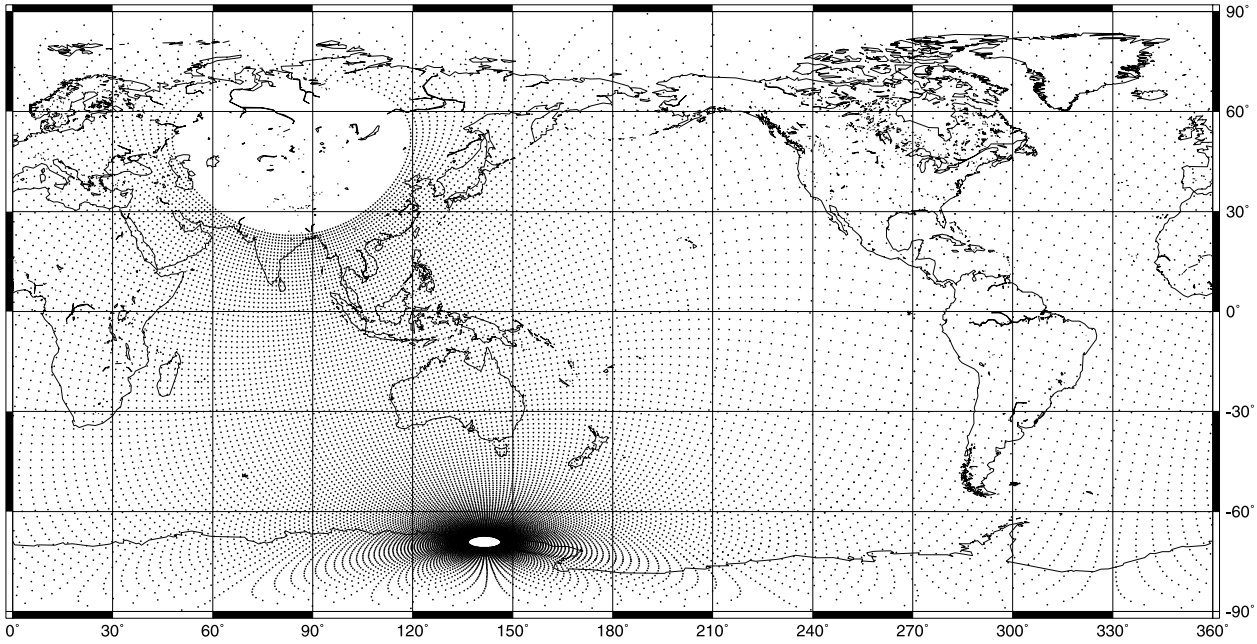

Figure 1. Geographical location of scalar grid points for the Mertz-HOPE model.

[8] We simulate ocean and sea ice processes in the MGP and Adélie Depression to determine the formation rate of dense shelf waters contributing to the production of ALBW. We examine interannual variability of the dense water formation and the relationship of this variability to the surface forcing and the ocean state. The paper is arranged as follows: A description of the model and forcing is given in section 2; in section 3, results from a 1991–2000 run with NCEP-NCAR daily forcing are shown; a discussion of the results appears in section 4.

2. Model and Forcing

[9] The model used in this study is the Arakawa C-grid [*Arakawa and Lamb*, 1977] version of the Hamburg Ocean Primitive Equation (HOPE) model. The grid used to study the Mertz region is known as Mertz-HOPE, and is a variant of the Max Planck Institute for Meteorology Ocean Model (MPIOM; as described by *Marsland et al.* [2003]). The HOPE model was originally written on an Arakawa E-grid and is documented by *Wolff et al.* [1997]. MPIOM has previously been used in studies of Arctic sea ice interaction with the North Atlantic [*Haak et al.*, 2003].

[10] MPIOM is a state-of-the-art hydrostatic Boussinesq primitive equation ocean model with z-coordinates on a spherical grid. The model includes a free surface elevation and partial vertical grid cells that fully resolve the discretized bottom topography. It has prognostic equations for horizontal velocities, pressure, temperature, and salinity. Additionally, there are subgridscale parameterizations of vertical and isopycnal diffusion, vertical and horizontal viscosity, eddy-induced mixing, bottom boundary layer transport, and open ocean convection. MPIOM includes an embedded sea ice model with viscous-plastic rheology [*Hibler*, 1979], zero-layer thermodynamics [*Semtner*, 1976], and a thermodynamic snow layer model including submerged snow to sea ice conversion. Hence the considerable insulating effects of snow accumulation on sea ice are included. The sea ice coverage is fractional within grid cells, and includes parameterizations of lateral and vertical ablation and accretion [*Stössel*, 1992]. See *Marsland et al.* [2003] for further details of the MPIOM (and Mertz-HOPE) equations, numerics, and performance, and see *Griffies et al.* [2000] for a description of z-coordinate OGCMs more generally.

[11] Figure 1 shows the location of grid points for the Mertz-HOPE model. A large-radius north pole lies over Eurasia, and a small-radius south pole is located inland of the MGP on the Adélie Land coastline. The grid is locally isotropic in the sense that the parallel and meridional grid distances are approximately equal within each grid cell. This constraint, in association with the variable pole sizes, results in the clustering of grid points about the smaller pole.

[12] Figure 2 shows the variable horizontal resolution. Resolution lies in the range 10–480 km, with the highest resolution in the East Antarctic sea ice zone from 120° to 150°. The model is everywhere non-eddy resolving, allowing for grid cell dependent subgridscale parameterizations of mixing, friction, and diffusion. Numerical parameters for the subgridscale processes are the same as used in MPIOM, and are detailed by *Marsland et al.* [2003]. It is reasonable to expect that these choices are appropriate, given that both Mertz-HOPE and MPIOM have similar ranges of variability in horizontal resolution.

[13] The Mertz-HOPE model was initialized with *Levitus et al.* [1998] objectively analyzed annual mean temperature and salinity data. The vertical discretization consists of 31 levels having thicknesses of 20, 20, 22.5, 25, 25, 25, 37.5, 50, 50, 75, 100, 100, 100, 100, 100, 100, 100, 100, 100, 100, 100, 150, 275, 375, 500, 500, 500, 500, 500, 500, and 750 m from top to bottom. These thicknesses were chosen so that the midpoints representing the model's z-coordinate levels coincide with the available *Levitus et al.* [1998] levels

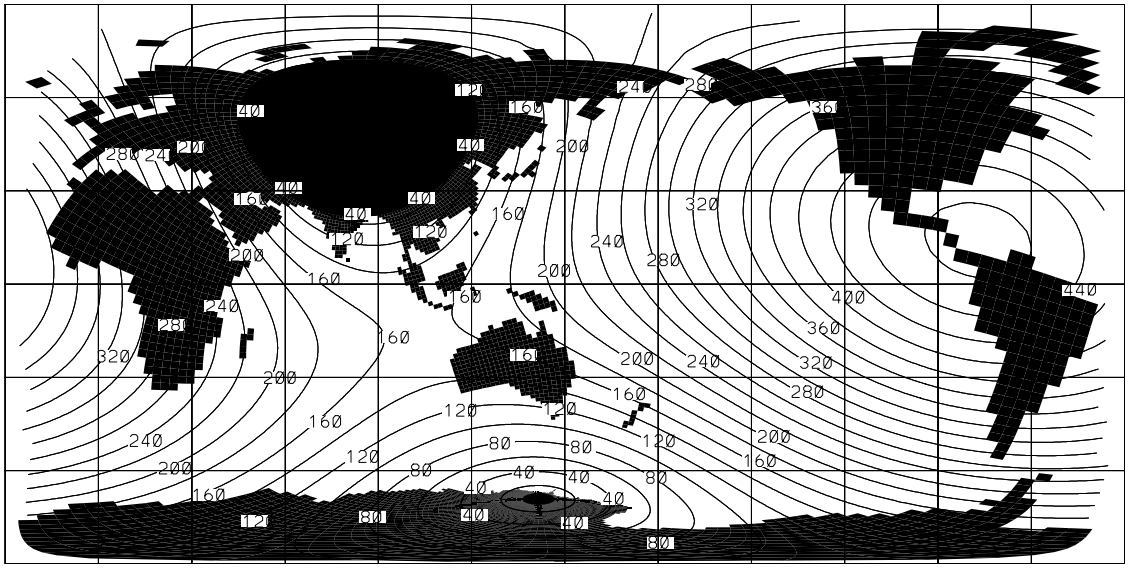

Figure 2. Horizontal resolution of the Mertz-HOPE setup. Contour interval is 20 km. The horizontal resolution ranges from 12 km in the Mertz region up to 475 km in the Caribbean Sea.

and emphasize the shallower depth range over the continental shelf needed to resolve the polynya processes.

[14] The geometry of the model's Adélie Depression is shown in Figure 3. For the purposes of this study, the MGT and the northward extension of grounded icebergs are represented by land points (white cells in Figure 3). There is a slight mismatch in the position of the Mertz Glacier when comparing the model (derived from the ETOPO5 digital atlas) to the GEBCO [*British Oceanographic Data Centre*, 1994] data set. In reality, the glacier tongue is floating, which allows for the flow of relatively warm ocean water beneath. Observations show that the resultant glacial melting results in the production of ISW [*Bindoff et al.*, 2001; *Williams and Bindoff*, 2003]. Currently, ocean-ice shelf interaction is not included in the Mertz-HOPE model.

[15] The model requires specification of the following prescribed forcing fields: air and dewpoint temperatures at the 2 m level; precipitation; normalized cloud cover; in-

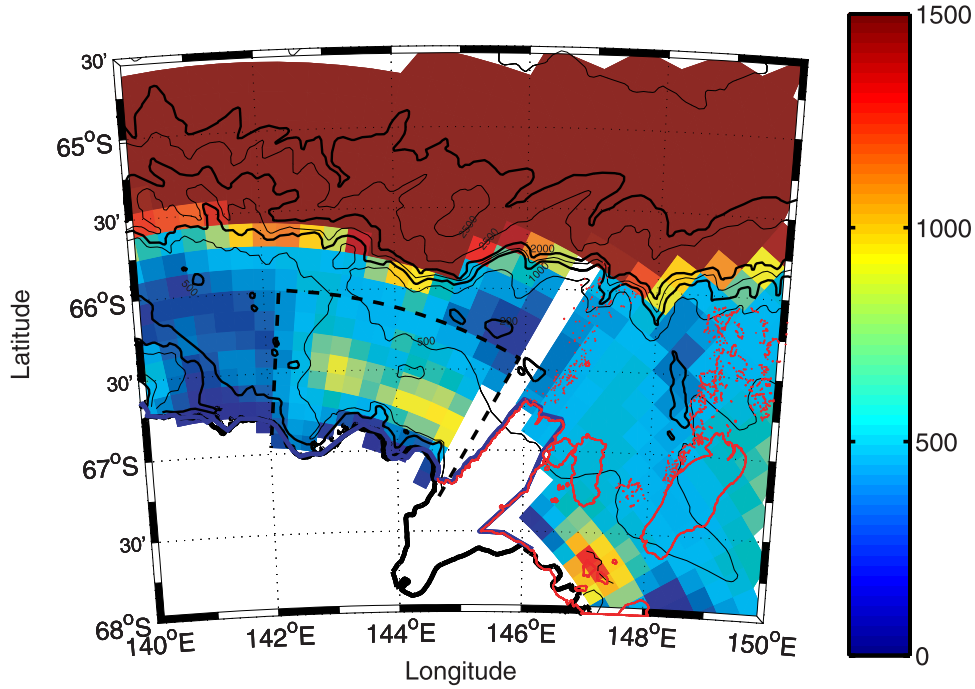

Figure 3. Model bathymetry in the region of the MGP and Adélie Depression (color cells). Black contours show bathymetric atlas contours [*British Oceanographic Data Centre*, 1994]. Red contours show the observed MGT and grounded icebergs. The black dashed line shows the region of our analysis box enclosing the Adélie Depression.

coming shortwave radiation; wind speed at the 10-m level; and surface wind stress. The model was spun up for 20 years using climatological surface forcing derived from the 1979–1993 ECMWF Re-analysis data set [*Gibson et al.*, 1997] as part of the German Ocean Model Intercomparison Project (OMIP) [*Röske*, 2001]. The OMIP forcing consists of a mean year with superimposed high-frequency (daily) synoptic scale variability. To explore interannual variability of the MGP and within the Adélie Depression, the integration was extended using NCEP-NCAR daily reanalysis fields [*Kalnay et al.*, 1996] for the period January 1990 until December 2000. Since there are considerable differences between the OMIP mean year and NCEP-NCAR reanalysis products (notably the incident shortwave radiation is around 10% greater in NCEP-NCAR), the change in forcing causes an initial shock to the modeled system. As the on-shelf ocean/sea ice system responds to the surface forcing relatively quickly, only the first year (1990) is excluded from our analysis. Results from the NCEP-NCAR daily forced run for the period 1991–2000 are presented in the next section. It is noted that both the ECMWF and NCEP-NCAR reanalysis products have serious inadequacies at high latitudes [*Simmons and Gibson*, 2000; *Kanamitsu et al.*, 2002]. Both were derived using satellite observed sea ice extents, but failed to incorporate realistic sea ice fractional coverage or thickness. This leads to large uncertainties in the heat flux components, a problem exacerbated by the poor treatment of clouds in atmospheric GCMs which leads to large errors in surface shortwave radiation. Although some of the problems of the forcing could possibly be avoided by choosing from different climatologies for each of the required surface forcing fields, it was deemed more beneficial to maintain consistency between forcing fields by choosing all forcing from one reanalysis product. This also allows for the use of consistent daily forcing: The importance of synoptic scale variability in modeling the Southern Ocean and sea ice system has been demonstrated by, for example, *Stössel* [1996].

[16] The net ocean to atmosphere heat balance equation is given by

$$Q_{\mathrm{net}} = Q_{\mathrm{se}} + Q_{\mathrm{la}} + Q_{\mathrm{lw}} + Q_{\mathrm{sw}}, \tag{1}$$

where Q_{se}, Q_{la}, Q_{lw}, and Q_{sw} are, respectively, parameterizations of the sensible, latent, longwave and shortwave components (defined to be positive upward).

$$Q_{\mathrm{se}} = \rho_a c_a C_H V_{10\mathrm{m}}(T_a - T_{\mathrm{srf}}) \tag{2}$$

$$Q_{\mathrm{la}} = \rho_a L_{\mathrm{srf}} C_L V_{10\mathrm{m}}(q_a - q_{\mathrm{srf}}) \tag{3}$$

$$Q_{\mathrm{lw}} = \varepsilon\sigma T_a^4\left(.39 - .05\sqrt{e/100}\right)\left(1 - \chi n^2\right) + 4\varepsilon\sigma T_a^3(T_{\mathrm{srf}} - T_a) \tag{4}$$

$$Q_{\mathrm{sw}} = (1 - \alpha_{\mathrm{srf}})Q_{\mathrm{incsw}}. \tag{5}$$

Each term is calculated separately for the sea ice covered and open water fractions of a model grid cell, and then a weighted average is determined according to the fractional sea ice coverage. The surface temperature T_{srf} is appropriately representative of open ocean, sea ice, or snow cover conditions. The 10-m wind speed $V_{10\mathrm{m}}$, 2-m air temperature T_a, fractional cloud cover n, and incident shortwave radiation Q_{incsw} are forcing terms derived from the NCEP-NCAR reanalysis daily data set. The air density ρ_a, air specific heat capacity c_a, latent heat of vaporization or sublimation L_{srf}, surface thermal emissivity ε, and Stefan-Boltzmann number σ are taken to be constant. Spatially variable C_H and C_L are, respectively, the linear coefficients of sensible and latent heat transfer from *Large and Pond* [1982]. The parameterizations of the specific humidities q and saturation vapor pressures e depend on water or sea ice/snow conditions and are calculated according to the formulae of *Buck* [1981]. The net longwave radiation parameterization follows that of *Berliand and Berliand* [1952]. The cloudiness factor χ is a modification based on work by *Budyko* [1974],

$$\chi = 0.5 + 0.4(\min(|\phi|, 60^\circ))/90^\circ, \tag{6}$$

with ϕ denoting latitude. The surface albedo α_{srf} is a constant representative of open water, sea ice, or snow cover. Separate values of albedo are used for melting or freezing conditions when ice or snow is present. When the surface air temperature is below freezing, precipitation is treated as snow which melts into open ocean and accumulates over sea ice. Further details are given by *Marsland et al.* [2003].

3. Results

[17] Validation of the Mertz-HOPE model output is sought by direct comparison with satellite and in situ observations. Figure 4 shows a typical pattern of sea ice in the region as observed by Advanced Very High Resolution Radiometer (AVHRR) channel 4 (thermal infrared; λ10.5 μm; approximately 1 km spatial resolution) satellite [*Massom et al.*, 2001]. From east to west can be seen the following: a fast ice blocking feature to sea ice advection following the westward flowing current associated with the Antarctic Slope Front (ASF) [*Whitworth et al.*, 1998]; the fast ice itself anchored by iceberg B9B and further icebergs to the north; a region of zonally trapped fast ice; the Mertz Glacier Tongue and northward extension of grounded icebergs; the Mertz Glacier Polynya as characterized by dark areas (open water and thin newly forming sea ice) in the lee of the MGT and extending west to Commonwealth Bay (143°E); and then an additional blocking feature to the west formed once more by grounded icebergs and fast ice. Sea ice vectors in Figure 4 are derived from buoy tracks [*Lytle et al.*, 2001] and satellite-tracked floes [*Massom et al.*, 2001]. Flow of sea ice from the MGP is generally to the northwest, with northward flow constrained by the thick ice that flows westward from the northern tip of the MGT.

[18] Simulated August 1999 mean sea ice fraction is shown in Figure 5a. Corresponding sea ice thickness is shown in Figure 5b. To the east of the MGT, there exists a wedge of sea ice with areal concentration approaching 100% and thickness increasing gradually from 1.5 m at 150°E to 3.0 m at 146°E. Immediately to the west of the MGT the model shows clearly a polynya with ice thickness in the range 30–50 cm and ice concentration reducing from

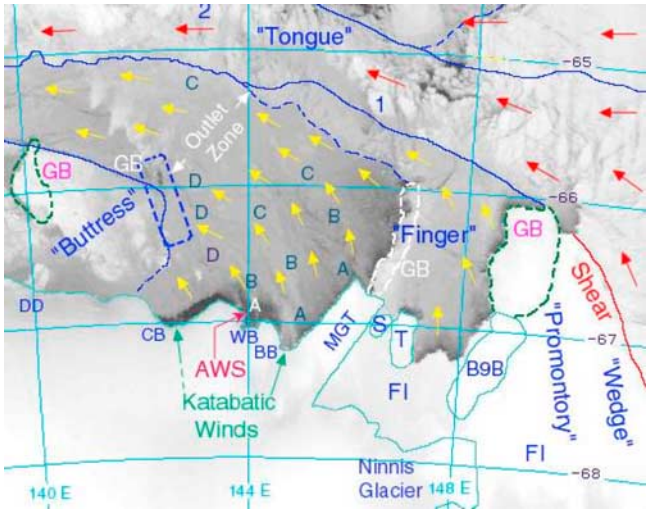

Figure 4. The Mertz Polynya region from an AVHRR image taken 14 July 1999. Abbreviations are as follows: grounded bergs (GB), fast ice (FI), iceberg B9B (B9B), grounded bergs (S and T), Buchanan Bay (BB), Watt Bay (WB), Commonwealth Bay (CB), and Dumont Dúrville (DD). Vectors are derived from buoy and satellite tracked floes, with yellow and red denoting new and old sea ice, respectively. For further details, see *Massom et al.* [2001].

northeast to southwest. Against the Antarctic coastline and the western edge of the MGT, sea ice concentrations fall below 40%. The model is also capable of reproducing the flow of thick sea ice flowing westward from the northern tip of the MGT. Also shown in Figure 5b is the mean July 1999 sea ice velocity field. To the east of the MGT, westward sea ice advection is deflected northward. To the west of the MGT the sea ice flow is predominantly westward.

[19] There are a number of similarities when comparing the observed sea ice of Figure 4 and the model product as shown in Figure 5. Extension of the MGP from the MGT as far west as Commonwealth Bay is in good agreement. Low sea ice thickness within the MGP is evident in both the model and the satellite observations, as is the tongue of thick sea ice advecting westward from the tip of the MGT. Sea ice speeds and directions are also in reasonable agreement, with higher speeds along the shelf break above the ASF.

[20] There are also a number of notable differences when comparing the Mertz-HOPE sea ice with the satellite observations. A variety of obstacles to sea ice flow are identifiable in the satellite picture that are not represented in the model. East of the MGT, iceberg B9B and the grounded bergs to its north are absent from the model, as is the promontory and wedge of fast sea ice farther east. There is no specific fast ice model included in the Mertz-HOPE model. However, it is reassuring that qualitatively the model is able to capture the process of the thick sea ice tongue at the tip of the MGT. Similarly, the grounded bergs at 140°E are absent from the model, along with the corresponding "buttress" of fast ice immediately to their east. It is also noted that the model sea ice velocities out of the MGP are more westward than the northwest direction interpreted from the AVHRR image and buoy tracks.

[21] Figure 6 shows the mean of Acoustic Doppler Current Profiler (ADCP) observed 100-m ocean velocity. Deeper depth levels have a lower signal-to-noise ratio in the acoustic signal from the ADCP instrument, and consequently maps of the circulation are poorer at 400 m than at 100 m. However, the ocean velocity is vertically coherent over the whole study region, and the estimated flow fields at 200 and 300 m are very similar to that shown at 100 m. The observed wintertime velocities are spatially sparse as the ADCP cannot be operated under ice breaking conditions. At around 66°S, there is a southward flow crossing the shelf into the Adélie Depression between 144°E and 146°E. This vertically coherent inflow across the shelf break carries Highly Modified Circumpolar Deep Water (HMCDW) into the depression and then turns southeast toward the MGT. At the intersection of the MGT and the Antarctic coastline, there is a westward return flow along the coastline, and an eventual northward outflow from the depression at 143°E. It is noted that there is considerable temporal variability in the observed velocities (not shown): This is associated with variability of inertial oscillations evident in the ADCP velocities, and also variability between the weeks when observations were repeated. One interesting feature of the subsurface (100 m) observed velocities is that the southeastward flow within the Adélie Depression is clearly opposite to the northwestward surface flow of the observed sea ice as evidenced in the buoy drift tracks [*Lytle et al.*, 2001]. The southward component of this flow is in mass balance with the northward component of wind-driven flow at the surface, and the northward export of dense water nearer the bottom of the depression; that is, water is drawn into the depression at intermediate depths. For further details of the ADCP velocities and water mass transformations, see the work by *Williams and Bindoff* [2003]. Also shown in Figure 6 is observed 100-m salinity. Although the observations are limited in spatial extent, they do show that fresher waters (<34.5 psu) are found off-shelf while saltier waters (>34.6 psu) are found within the polynya region and are more salty to the west.

[22] For comparison with the observed 100-m velocity and salinity fields the Mertz-HOPE model output is shown in Figure 7a. High salinities (>34.6 psu) to the north of the ASF are associated with upwelling Circumpolar Deep Water and are in a region of relatively quiescent flow. Strongest flow is along the shelf break and is westward, approximately following the bathymetry. South of the shelf break the meridional component of the flow is predominantly southward, providing an inflow to the Adélie Depression. Within the MGP region the flow is southeastward and toward the MGT. A narrow westward return flow along the Adélie Coast can be seen at both 100- and 400-m depth levels (Figure 7). This westward flow along the coast feeds a northward outflow (bounded by bathymetry to the west at 400 m) from the Adélie Depression where the sill depth is a maximum (66°S, 143°E). The outflowing current appears to be boundary intensified along the western edge of the Adélie Depression between 66°S and 67°S.

[23] Comparison of Figures 6 and 7a is difficult because of the sparsity of the observations. The wintertime observations show fresh waters to the north and increasing salinity toward Antarctica. The model salinity field is similar, although notably fresher immediately west of the

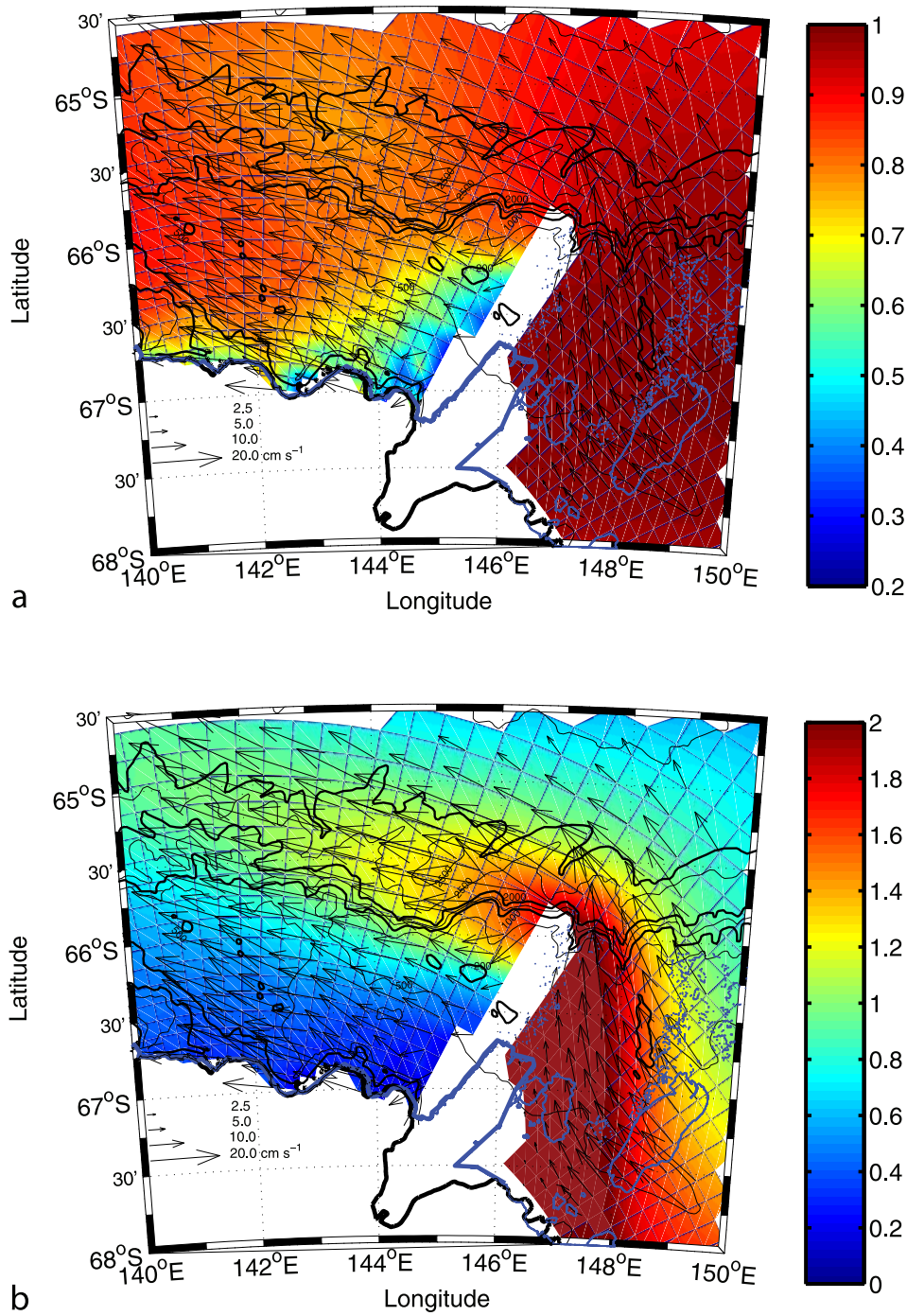

Figure 5. Modeled mean monthly (a) normalized sea ice fraction and (b) sea ice thickness (m) for August of 1999. Black contours show GEBCO [*British Oceanographic Data Centre*, 1994] bathymetry. The dark blue line denotes the actual position of the MGT, as well as grounded bergs to the north and east of the MGT. Vectors show the corresponding mean monthly sea ice velocities (cm s^{-1}).

MGT where bathymetry is shallower than 500 m. This is attributed to the freshwater input from melting of thick sea ice to the east of the MGT, where the model does not simulate fast sea ice. The model shows that the salinity increases as the flow moves toward the MGT and is higher along the Antarctic coastline with a maximum in the region of Commonwealth Bay. Qualitatively, the model pattern of salinity is consistent with the limited observations during winter. Direct observations of salinity in Commonwealth Bay during a summertime cruise of the *Nathaniel B. Palmer* also show the highest values are seen in this region (Stan Jacobs, personal communication, 2002), as is inferred from the wintertime measurements [*Williams and Bindoff*, 2003]. The model simulates an overall pattern of a conveyor belt moving water toward the MGT at 100 m, and then westward as a narrow current along the Adélie coastline at depths of

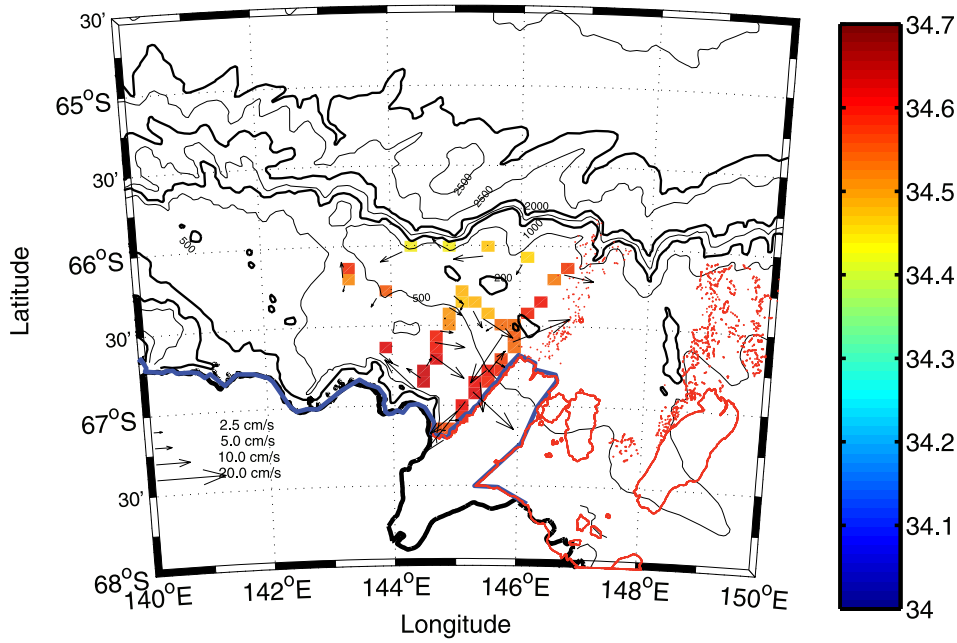

Figure 6. Vectors show ADCP observed velocity at 100 m depth (cm s^{-1}) in July/August of 1999. Also shown is the observed 100 m depth salinity (psu).

100 and 400 m, with progressively increasing salinity resulting from intense air-sea interaction. Qualitatively, this is the same overall circulation inferred by *Williams and Bindoff* [2003] from relatively sparse observations of water masses and currents.

[24] A number of drifting buoy arrays were deployed during the winter 1999 experiment [*Lytle et al.*, 2001]. Figure 8 shows a typical comparison of observed average daily buoy speed (top) and heading (bottom) with interpolated model drift. Buoy C was deployed at the tip of the Mertz Glacier (146°E, 66.7°S), which is equivalent to about halfway along the model boundary, representing the MGT and northward iceberg extension. It drifted in a west-northwest direction to a final position at approximately 138°E, 65°S. This drift pattern was typical of the 17 buoy deployments during the experiment. Both the magnitude and variability of the model sea ice speed are in good agreement with the buoy observations. It is clear that the model sea ice is responding to the same weather systems as the actual buoys. There is no systematic bias between model speed and buoy speed. Comparison with the model sea ice vectors shows an anticlockwise bias toward the west (i.e., too weak a northerly component) of around 15°. Comparison of the drifting buoy tracks with derived buoy tracks from the model confirms this bias (Matthew Paget, personal communication, 2003), which can be partially attributed to the absence of fast ice in the west of the Adélie Depression. Further confidence in the model's response to synoptic weather systems is the 1999 anomalous late season breakout of sea ice in the region (not shown) as observed by *Massom et al.* [2003].

[25] Figure 9 shows a north-south section of mean August salinity over the period 1991–2000. North of 63°S, isohalines slope downward from south to north, and are geostrophically associated with the mean eastward flow of the southern limb of the Antarctic Circumpolar Current (ACC). Over the region 64°S–66°S, isohalines slope downward from north to south, indicating the westward flowing coastal counter current. The transitional shear zone can be seen as doming of the isohalines in the region 63°S–64°S. Over the southern side of the Adélie Depression (66°S–67°S) the isohalines also have negative slope. This is consistent with a westward Ekman flow driven by strong northern wind stress. This current is boundary intensified due to the downward component of the vertical velocity. Consequently, the isohalines form a distinctive V-shape (65°S–67°S) in the upper 500 m. Such a V-shape, indicative of dense shelf water formation driven by intense surface buoyancy forcing, was first noted in the Weddell Sea by *Gill* [1973]. He identified it as a characteristic feature for source regions of AABW. The V-shape was also observed in the Ross Sea by *Ainley and Jacobs* [1981] and identified as the Antarctic Slope Front (ASF), and along the East Antarctic coast between 140°E and 150°E [*Rintoul*, 1998; *Bindoff et al.*, 2000]. Within the V-shape lies a westward flowing layer of relatively cold and fresh water that *Deacon* [1937] refers to as the near-circumpolar East Wind Drift. The ASF is further described by, for example, *Jacobs* [1991] and *Whitworth et al.* [1998].

[26] One measure of the buoyancy forcing that drives the HSSW formation is the brine rejection caused by the growth of sea ice. The time integral of divergence of sea ice transport γ is given by

$$\gamma = \int_t \nabla \cdot (h_i \vec{v}_i) dt, \tag{7}$$

where t is time, $\nabla = \frac{\partial u}{\partial \lambda} + \frac{\partial v}{\partial \phi}$ is the divergence operator, h_i is the local sea ice thickness, and $\vec{v}_i = (u, v)$ is the local sea ice

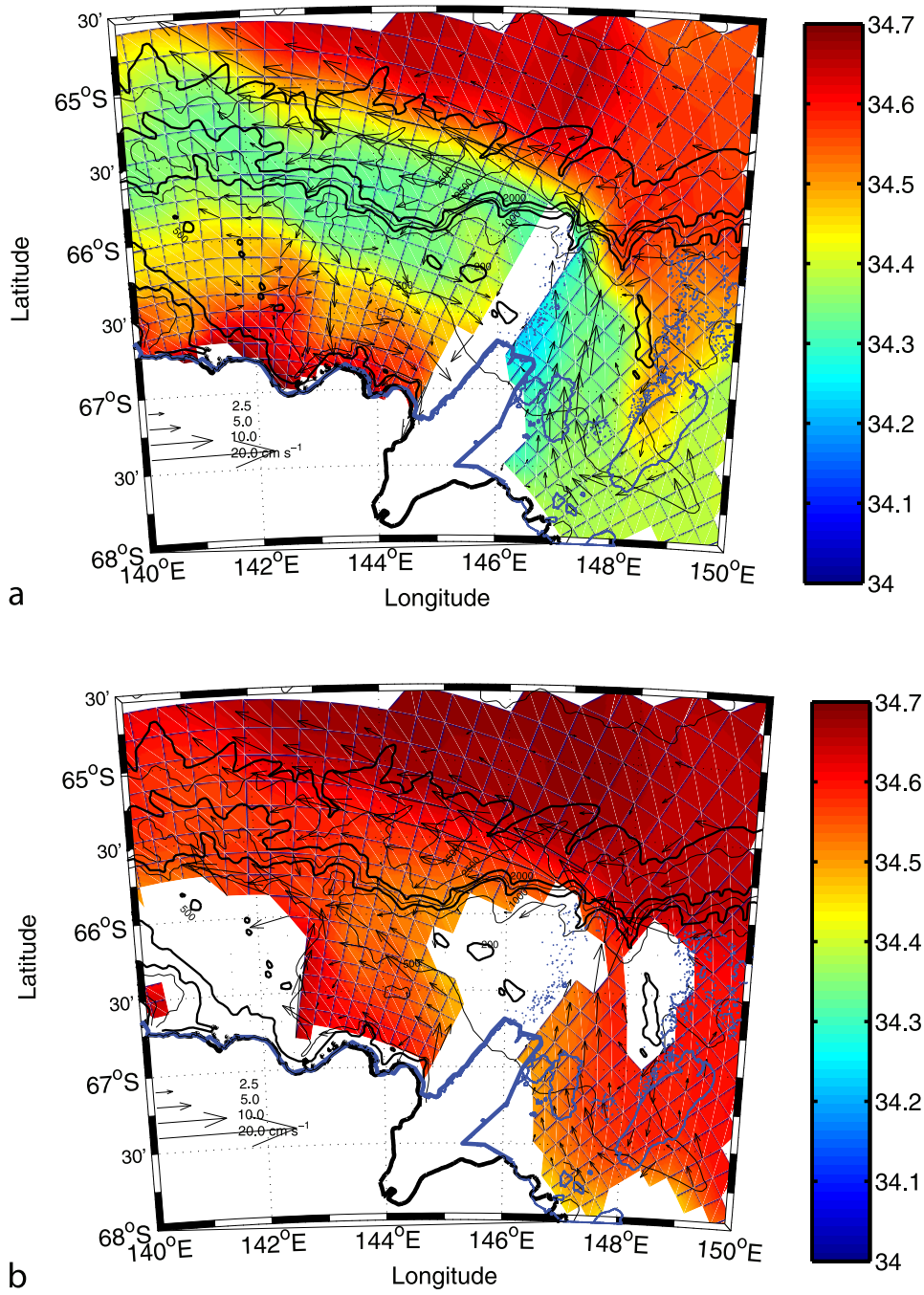

Figure 7. As in Figure 6, but for the Mertz-HOPE model at (a) 100 m and (b) 400 m depths.

velocity. Here the parallel and meridional directions (velocities) on the orthogonal curvilinear grid are represented by λ and ϕ (u and v), respectively. The integral over the decade 1991–2000 is shown in Figure 10, and is a direct measure of local sea ice growth or melt over the model domain. The net sea ice growth rate is up to 10 m yr^{-1} along the eastern edge of the MGT, and also along the Antarctic coastline within the Adélie Depression. This is consistent with the heat flux observations of *Roberts et al.* [2001], who suggest that this inner part of the MGP has a very high ice production rate. Most of the sea ice formed in the polynya and along the coast is advected northward so that much of the region north of 64°S has annual net ice melt. That is, given sufficiently high horizontal resolution, the Mertz-HOPE GCM favors sea ice growth near shore and sea ice melt off shore. This is an important consideration for coarser resolution GCMs that in general do not have sufficient resolution to capture this process. The sea ice divergence was integrated over the region covering the Adélie Depression (see dashed box in Figure 3) for the period of high sea ice growth rates (May through September inclusive). The mean wintertime sea ice growth is 7.5 m yr^{-1} at a rate of 4.9 cm d^{-1}, the same rate as found by *Bindoff et al.* [2000]. This is also in reasonable agreement with the

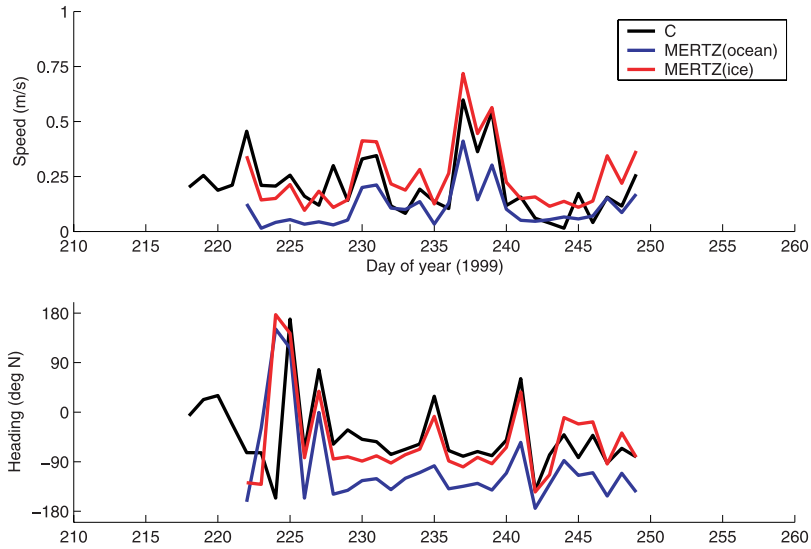

Figure 8. Comparison of observed Buoy C speed and heading with speed and heading interpolated from the Mertz-HOPE model for the duration of the 1999 Mertz Polynya Experiment.

estimate of 5.8 cm d^{-1} of *Williams and Bindoff* [2003], and the directly observed growth rate of 4.0 cm d^{-1} for columnar sea ice [*Lytle et al.*, 2001]. The box has a surface area of 13,143 km^2, so the model results in the average annual production of 98.7 km^3 of sea ice over the Adélie Depression.

[27] We use an index to describe the polynya as a region of high sea ice production and open water fraction. This allows us to discriminate from other open water regions with low sea ice production, such as the marginal ice zone at the northern edge of the sea ice. Our index for identification of the model's MGP is formed by choosing those grid cells that have both low sea ice concentration (<70%), and high sea ice production as defined by equation (7) (>1 m $month^{-1}$). Figure 11a shows the mean monthly integrals of this defined polynya area. Also shown is the mean monthly ice free area within the polynya as determined from the mean monthly sea ice concentrations, and the wintertime (defined as May to September inclusive) averages of these areas. The annual ratios of wintertime ice free area to winter time polynya area lie between 0.50 and 0.57. That is, the indexed MGP is on average at least 50% ice free. The wintertime average polynya area is in the range 10,000–13,000 km^2 for all years considered except for

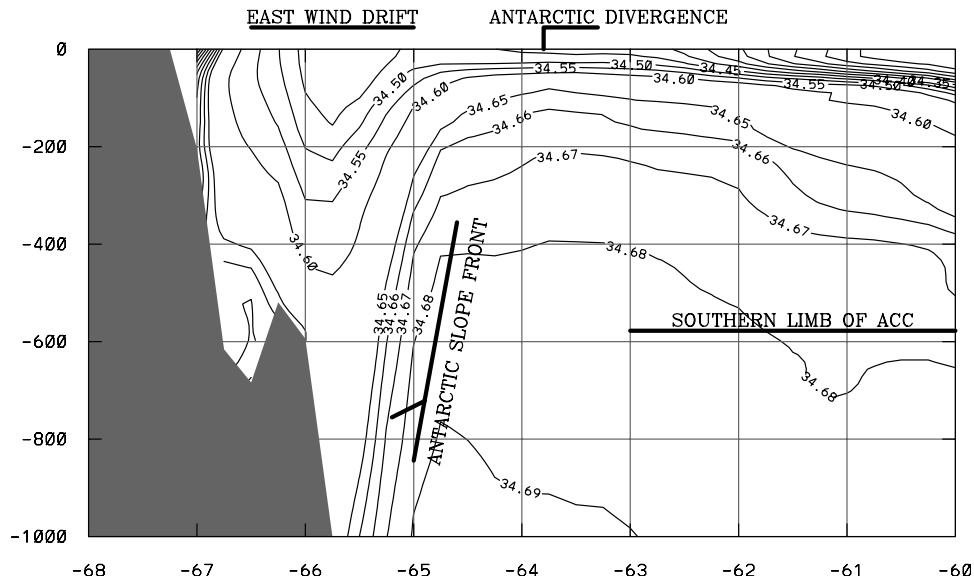

Figure 9. Mean August section of model salinity (psu) along 143°E for the period 1991–2000. Note that the contour interval is 0.05 below salinities of 34.65 and 0.01 above salinities of 34.65. Labels show depth (ordinate) and latitude (abscissa).

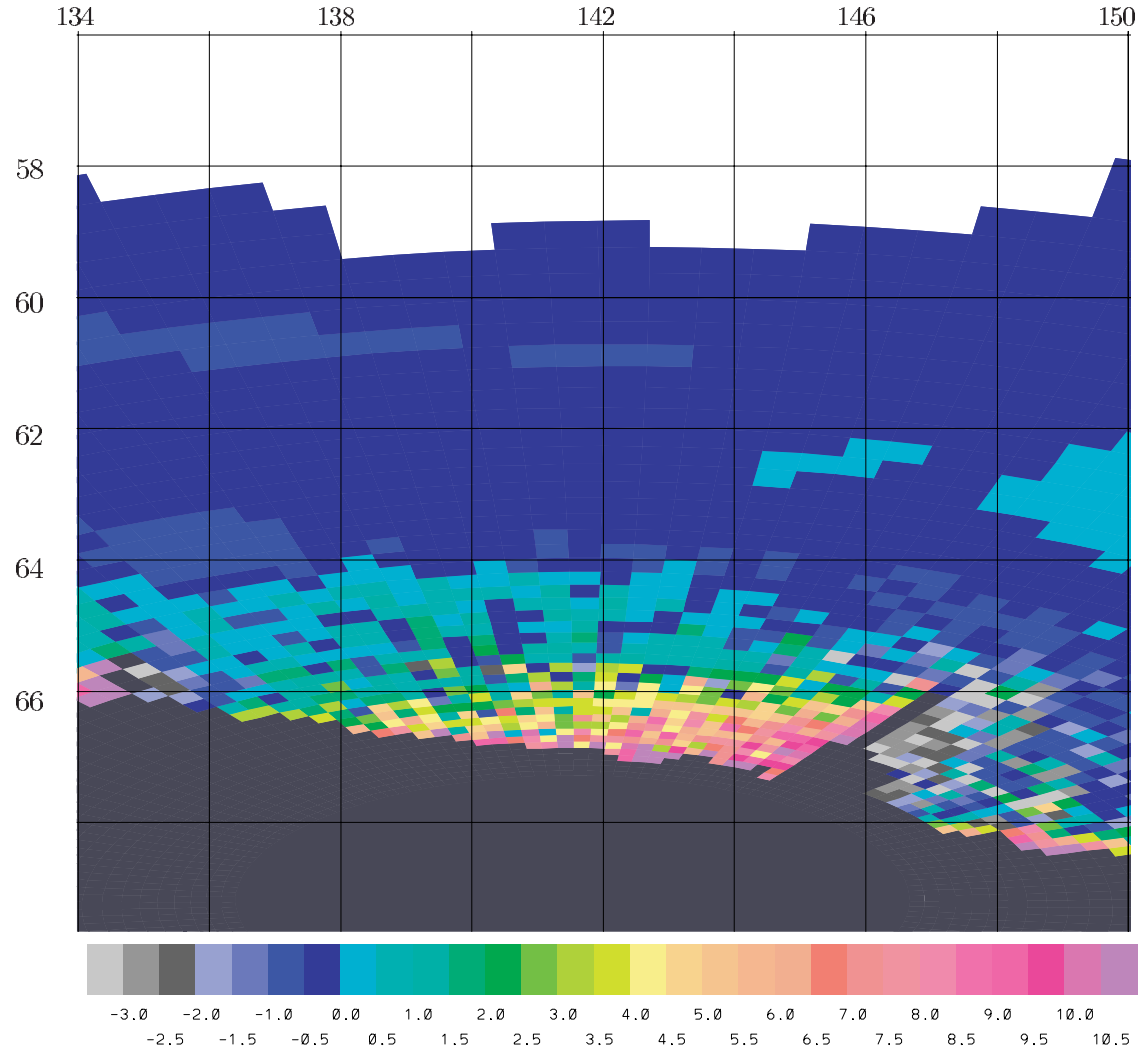

Figure 10. Divergence of sea ice transport (m) integrated over the period 1991–2000. Positive values denote regions of net sea ice growth, while negative values denote regions of net sea ice melt.

1991 and 1994, when this size falls below 10,000 km^2. This is somewhat smaller than the average winter size of 23,300 km^2, using a 75% ice concentration criterion and satellite observations [*Massom et al.*, 1998]. However, the observed quantity was derived only from areal concentration of the sea ice, while our indexing is more discriminating about the thermodynamically active state of the defined MGP. The modeled MGP persists through all the winters considered, which is also consistent with observation; *Massom et al.* [1998] reported a MGP for all 37 months that they considered. Of the 27 other East Antarctic polynyas they studied, they note that only the Shackleton Ice Shelf polynya is as persistent. The largest model MGP size of slightly over 15,000 km^2 occurs in both 1993 and 1997, and occurs early in the season. This contrasts with *Massom et al.* [1998], who report maximum size in October, but once again, this could be a consequence of the different approaches to determining the size.

[28] Figure 11b shows time series of mean monthly atmosphere to ocean surface heat fluxes and the average wintertime (also May to September inclusive) net heat flux (equation (1)), over the polynya region as indexed in Figure 11a. It can be seen in Figure 11b that the net heat flux is dominated by the sensible heat flux (equation (2)). The wintertime net heat flux shows considerable interannual variability. It lies in the range 175–200 W m^{-2} in low years (1991, 1992, 1999, 2000) and 200–250 W m^{-2} in high years (1993 through 1998 inclusive). Direct observation of the turbulent heat fluxes in the MGP is limited to two 30-km helicopter transects near the coastline [*Roberts et al.*, 2001]. On the transect characterized by a high (low) wind speed of 20 m s^{-1} (5 m s^{-1}), they found the sensible and latent heat fluxes to average 460 (201) and 114 W m^{-2} (48 W m^{-2}), respectively. Although very limited, these observations support the model result that sensible heat loss dominates latent heat loss close to the coastline, where the open water fraction is larger and the polynya seems most active in terms of higher wind speeds and greater sea ice production rate.

[29] In the Mertz-HOPE model the wintertime latent heat flux over the indexed MGP is 39 W m^{-2}. Two studies have produced indirect estimates of the latent heat flux in the

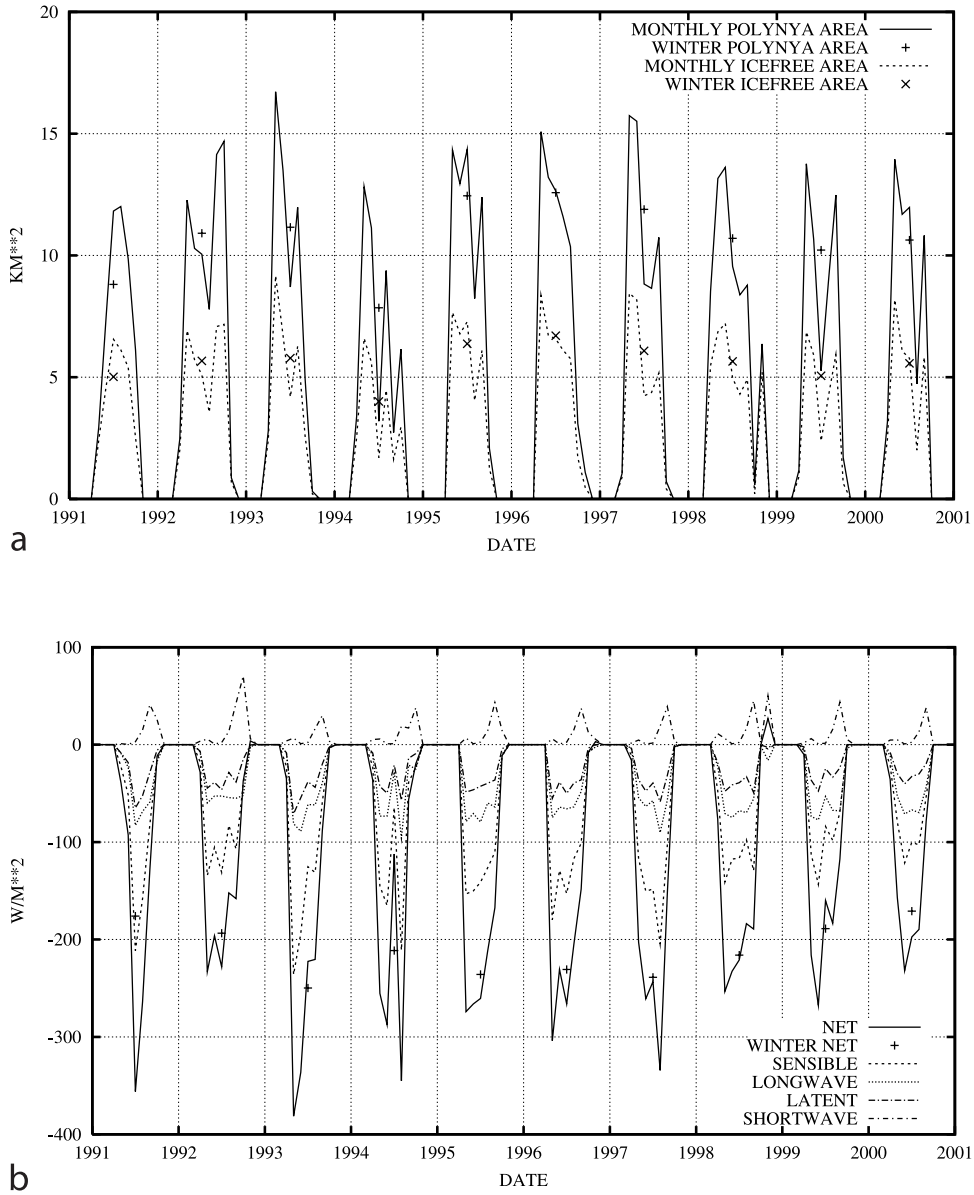

Figure 11. Time series of (a) mean monthly polynya area and ice free area within the polynya and (b) atmosphere to ocean surface heat fluxes within the polynya for the years 1991–2000 inclusive. The ordinate is labeled in units of 1000 km^2 for areas, and in W m^{-2} for fluxes. Abscissa labels show start of year. Also shown are the winter (May through September inclusive) means for the areas and for the net heat flux. The polynya is defined as the region having sea ice concentration less than 70% and local sea ice production greater than 1 m $month^{-1}$.

MGP based on hydrographic observations. *Bindoff et al.* [2001] used a simple model based on the zonal velocities of the observed water masses on a section adjacent to the MGT. They found a latent heat flux of 71 W m^{-2} was required to account for the 4.9 cm d^{-1} of sea ice growth, at least for the period of the 1999 Mertz Polynya Observational Experiment. However, that result is quite sensitive to an arbitrary choice of open water fraction. They choose an open water fraction of 20% which is considerably smaller than the 50% open water in our modeled MGP. *Williams and Bindoff* [2003] calculate the salt divergences around a closed volume bounded by three CTD sections and the Antarctic coastline to estimate the sea ice growth rate (5.8 cm d^{-1}) and the corresponding latent heat flux (174 W m^{-2}). As mentioned above, the Mertz-HOPE model has a high open water fraction (>50%), leading to a higher proportion of heat loss as sensible heat. This helps to explain the discrepancy between model and observation derived latent heat estimates.

[30] To investigate the on-off shelf exchange of water masses, a box was constructed bounded on the south by Antarctica, on the east by the MGT, on the west by a section following a model orthogonal curvilinear meridian at approximately 142.5°E, and on the north by a section following a model orthogonal curvilinear parallel at approximately 66.25°S. This box (see Figure 3) encloses the model Adélie

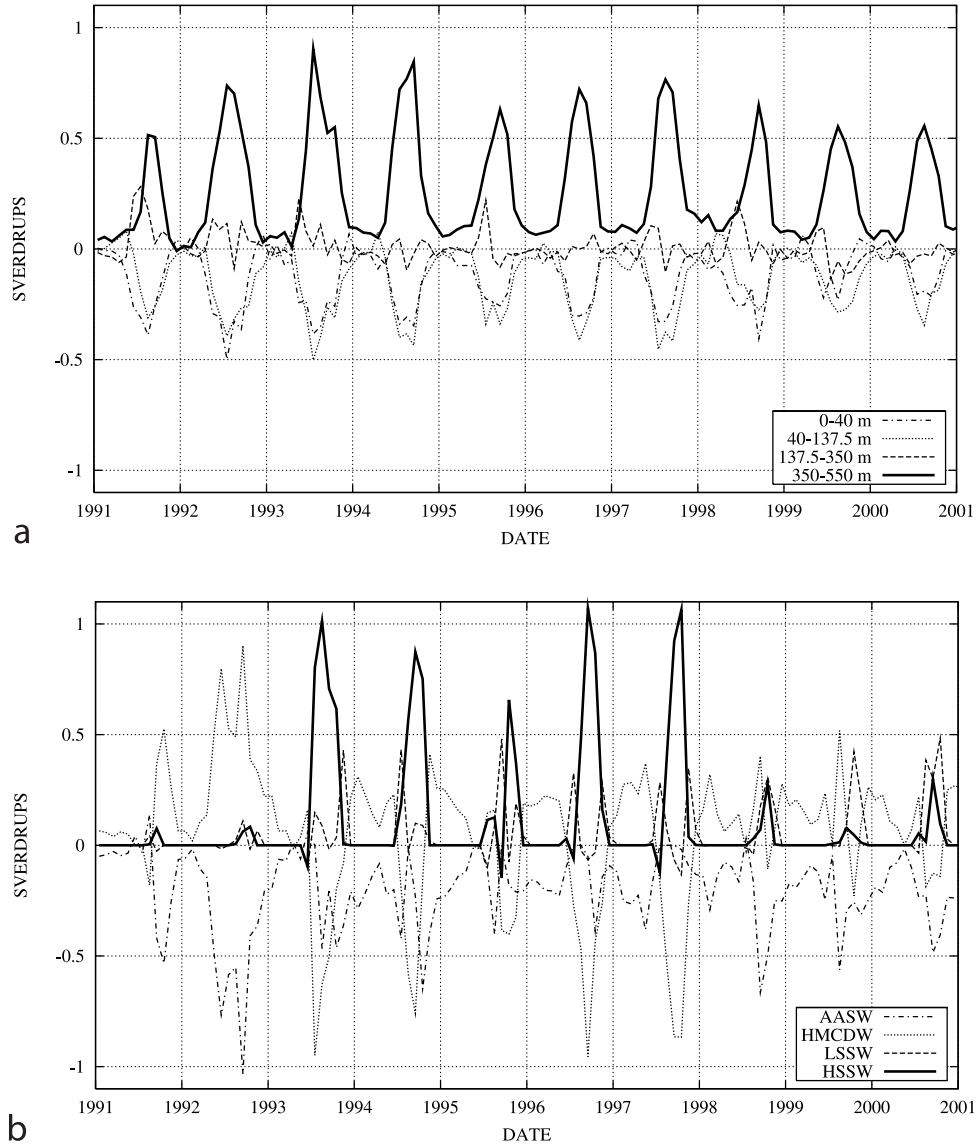

Figure 12. On-shelf (negative) and off-shelf (positive) water mass exchange (Sv) (a) for model *z*-coordinate levels and (b) for selected density classes. Density classifications are Antarctic Surface Water (AASW, $\sigma < 27.78$); Highly Modified Circumpolar Deep Water (HMCDW, $27.78 < \sigma < 27.88$); Low Salinity Shelf Water (LSSW, $27.88 < \sigma < 27.91$); and High Salinity Shelf Water (HSSW, $27.91 < \sigma$). Labels show flow in Sv (ordinate) and start of year (abscissa).

Depression. Figure 12a shows the water mass exchange into and out of this box on model *z*-coordinate levels. Figure 12b shows the water mass exchange into and out of this box on selected density levels chosen after *Bindoff et al.* [2001]. It can be seen in Figure 12a that in general, waters enter the Adélie Depression near the surface (40–350 m) and leave at depth (350–550 m). The on-/off-shelf flow on model levels shows a strong seasonal cycle, with the mass flux peaking in the winter months. This suggests that the cross-shelf exchange of waters is driven largely by the buoyancy forcing. Further, these mass fluxes are relatively uniform between years, with the peak outflow ranging between 0.5 and 1.0 Sv. However, the density structure of these waters exhibit considerable interannual variability, as shown in Figure 12b. In particular the outflow of HSSW, the densest class considered and the most likely contributor to AABW formation, has large peaks in some years, but is virtually nonexistent in others.

[31] Comparison of the interannual peaks of HSSW (Figure 12b) with the net surface heat flux (Figure 11b) suggests that there were two distinct regimes of polynya activity during the 1990s. The period 1993 through 1997 inclusive is characterized by high heat flux and greater export of HSSW off the continental shelf. The other years are characterized by lower heat flux and lower HSSW production. The years of high HSSW outflow are coincident with high HMCDW inflow into the depression. In years of low HSSW production, the cross-shelf exchange is better characterized by outflow in our HMCDW class, and inflow in our AASW class (e.g., 1992). The mean outflow of HSSW (LSSW) from the Adélie Depression averaged over the years 1991–2000 is 0.11 (0.05) Sv. Most of this

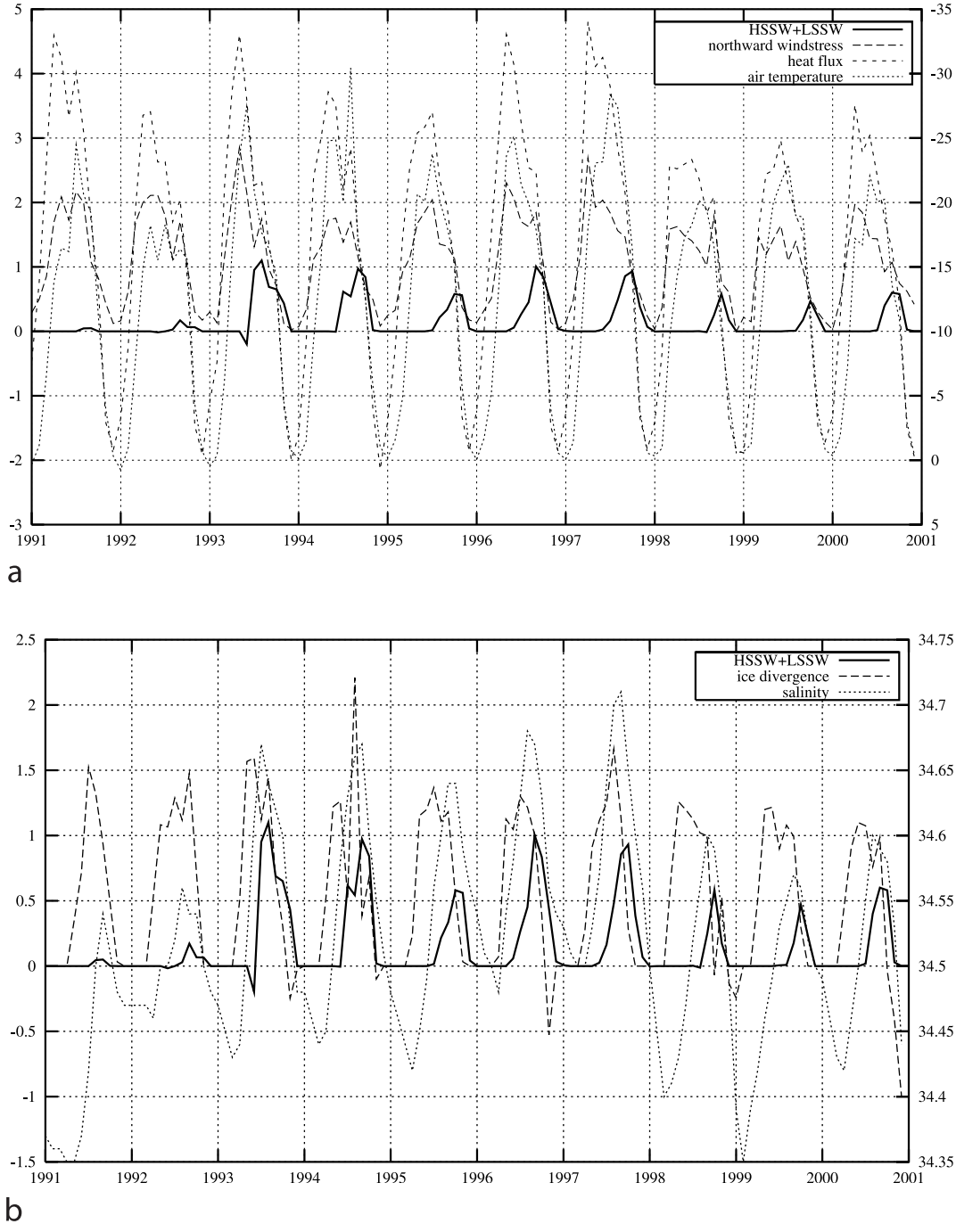

Figure 13. Time series comparison of dense water outflow rate with integrated quantities over the Adélie Depression for the period 1991–2000 inclusive: (a) HSSW + LSSW (Sv, left ordinate), northward wind stress (Pa × 10, left ordinate), net ocean to atmosphere heat flux (W $m^{-2} \times 10^{-2}$, left ordinate), and surface air temperature (°C, right ordinate); (b) HSSW + LSSW (Sv, left ordinate), net sea ice divergence (m $month^{-1}$, left ordinate), and volume integrated salinity from surface to bottom (psu, right ordinate).

exchange occurs in the months July through October when the decadal average HSSW (LSSW) outflow rate is 0.30 (0.10) Sv. For the 1993–1997 period of strong polynya activity, the annual average of HSSW outflow rises to 0.19 Sv, while the LSSW outflow remains unchanged at 0.05 Sv. Over the same period, the July–October average of HSSW (LSSW) production is 0.55 (0.08) Sv. Considering the combined outflow of both HSSW and LSSW, since both are sufficiently dense to be potential sources of ALBW [*Bindoff et al.*, 2001], the annual average dense shelf water outflow rate is 0.15 Sv over the period 1991–2000, and 0.24 Sv over the period 1993–1997.

[32] Figure 13a shows the relationship of the outflow of dense waters (HSSW+LSSW) from the Adélie Depression with the surface forcing (northward wind stress, ocean to atmosphere heat flux, surface air temperature). Figure 13b

shows the corresponding relationship with the ocean/sea ice state (sea ice divergence, depth-averaged salinity). All of these quantities are derived for the box shown in Figure 3. The response of the polynya to the atmospheric and oceanic forcing shows a strong seasonal cycle. Superimposed on this seasonal cycle, there is a distinctive interannual variation in the polynya processes, particularly in the oceanic parameters of volume-averaged salinity and the fluxes of dense water out of the control volume.

[33] Comparing the ocean parameters (salinity, and HSSW + LSSW fluxes out of the closed volume) with the surface atmospheric parameters indicates that the coupled response of the three systems (ocean, sea ice, ''atmosphere'') is important to the overall bottom water production. The production of dense shelf waters depends to some extent on the previous history of the shelf waters. For example, in 1996 and 1997 the austral autumn salinity is high in the Adélie Depression, as is the wintertime salinity and the production rates of dense shelf waters. By contrast, the autumn (and winter) salinities in the later years (1998, 1999, and 2000) are much lower leading to the lower and later production rates of dense shelf waters.

[34] These pronounced interannual variations lead to the question of what controls the autumn salinity values in the coupled system. The factors that exert influence over the ocean salinity are, of course, the seasonal ice divergence (and hence brine production), the seasonal divergence of salinity, and the storage terms for salinity on the shelf. The values of the salinity in the autumn period are related to the melt cycle of sea ice and the accumulation of fresh water along the Antarctic coastline during the summer months. Years of lower northward transport of ice from the shelf area will lead to high levels of melt and lower summertime salinity values over the shelf. The low autumn salinity values lead to increased stratification, and more work is required by the heat loss and ice divergence in the polynya to build the salinity up over the depression to the high values required to make the dense shelf waters required for bottom water. The 1998, 1999, and 2000 years are characterized by weak offshore winds (and lower heat fluxes) relative to the 1993–1997 period. This is consistent with the importance of the northward transport of ice during the summer months in producing the high autumn salinities required for HSSW production in the Adélie Depression.

4. Discussion

[35] Sea ice production in the MGP, along with the associated dense water formation in the Adélie Depression, is believed to be an important source of ALBW [*Rintoul*, 1998]. This has led to a number of recent observational studies of the region in both summertime [*Fukamachi et al.*, 2000] and wintertime [*Williams and Bindoff*, 2003]. This study is the first attempt at high-resolution general circulation modeling of the coupled ocean and sea ice processes within the MGP and Adélie Depression. The Mertz-HOPE setup has non-equal radii of the polar singularities, which, in conjunction with the grid quadrature (i.e., zonal and meridional grid distances locally equal), produces high horizontal resolution in our region of interest. Of course, it would have been possible to obtain the necessary high resolution using more traditional latitude-longitude grids. However, to do so on a global scale would be too computationally expensive, while to apply a regional model would introduce the nontrivial problems of either open or closed boundary conditions. Our knowledge of the hydrography and ocean currents of the Southern Ocean is inadequate to accurately determine such vertical boundary conditions, and thus it would be less likely to create realistic ocean circulations near the MGP. The Mertz-HOPE horizontal grid is an innovative approach that avoids both of these problems.

[36] We find that the Mertz-HOPE model is capable of reproducing the observed features of the MGP and Adélie Depression, along with the adjacent East Antarctic upper ocean and sea ice system. In particular, the thickness and areal concentration of the large scale pack ice, the size and location of the MGP within the pack, and the westward flow of a tongue of thick ice from the tip of the MGT are all in good agreement with observations. Although hardly surprising, it is of course reassuring that the Mertz-HOPE model simulation under NCEP-NCAR daily forcing results in a MGP of realistic location. Over the period 1991–2000 the modeled MGP has a wintertime (May–September) area of 10,000–15,000 km^2, exhibiting low ice thickness (<0.04 m), low ice fraction (<50%), and high ice formation rates (7.5 m yr^{-1} averaged over the Adélie Depression).

[37] It was found that most of the sea ice formation in the region occurs within a narrow band along the coastline, and the high resolution is indeed necessary for capturing this process: Experiments with MPIOM at 3° and 1.5° resolution do not show a MGP, and it is unclear how to parameterize this sharp transition in coarser resolution ocean climate models. The time integration of the divergence of sea ice transport shows that the highest growth rates are to be found within one or two grid cells (<30 km) from the Antarctic coastline. Over the Adélie Depression an annual average of approximately 100 km^3 of sea ice is formed. The Southern Ocean sea ice area is approximately 15 million square kilometers. Assuming a mean sea ice thickness of half a meter, the MGP then produces around 1.3% of the Southern Ocean sea ice volume, in a region of less than 0.1% of the total sea ice extent around Antarctica. For comparison, the Terra Nova Bay polynya in the Ross Sea is believed to produce around 50–80 km^3 of sea ice, albeit at a higher growth rate of 40–60 m $year^{-1}$ over a smaller area of 1000 km^2 [e.g., see *Morales Maqueda et al.*, 2004]. This volume of sea ice production in the Terra Nova Bay polynya represents 10% of the total production over the Ross Sea continental shelves [*Kurtz and Bromwich*, 1985]. Clearly, regions such as the MGP and Terra Nova Bay polynya are important regions of sea ice production in the Southern Ocean. We also find that the net northward sea ice export results in annually averaged sea ice melt over much of the region north of 64°S, which is known to provide a strong stabilizing buoyancy force via freshwater input to the upper ocean [*Marsland and Wolff*, 2001]. The net freshwater effect of the northward sea ice advection is equivalent to a 50% increase in the precipitation over the off-shelf pack ice. It is worth noting that the ice shelf melting, which is not included in this study, would add to the freshwater export from the depression: For example, *Timmermann et al.*

[2001] find the ice shelf melt component to be of a similar magnitude to the precipitation in their model study of the Weddell Sea. Hence, not only is the MGP an important source region of dense water formation, the freshwater export by sea ice advection from the MGP also acts to reduce the effectiveness of the surrounding sea ice region in driving dense water formation.

[38] Off the shelf the ocean currents realistically capture the main features of the southern limb of the eastward flowing ACC, a westward flowing ASF, along with the characteristic V-shape of isopycnals indicative of dense water formation and downslope propagation (Figure 9). Within the depression, the model velocities show an approximate clockwise circulating flow. We infer an open-ended conveyor belt-like circulation. A northern front is characterized by southward intrusion of HMCDW onto the shelf and then eastward flow toward the MGT. This subsurface HMCDW intrusion is counter to the northwestward sea ice drift in both the model and observations. Salinification occurs along the southern limb of the gyre, with the highest salinities occurring in the westernmost region of the Adélie Depression at Commonwealth Bay. We found that the on-/off-shelf exchange of water masses exhibits a strong seasonal cycle, with stronger exchange during the winter months and weaker exchange during the summer months. While this cycle is in phase with the seasonality of the northward wind stress, the southerly component of the HMCDW intrusion suggests that it is actually the buoyancy forcing that is driving the cross-shelf exchange of water masses.

[39] The region of highest salinity is located directly south of the deepest outlet from the Adélie Depression, and it is here that the HSSW is most easily able to flow off the shelf. Although the cross-shelf exchange is relatively constant from year to year, we find marked differences in the HSSW outflow between states of active versus relatively inactive years. That is, the interannual variability that we find in the model is manifested as variability in water mass classification (density) rather than variability in net volumetric exchange. During the more active period (1993–1997) the system is characterized by outflow of HSSW with an associated inflow of HMCDW. During the less active periods (1991–1992, 1998–2000) the system is characterized by outflow of LSSW with an associated inflow of AASW. From lightest to densest, these classes are ordered as AASW, HMCDW, LSSW, and HSSW. Thus in the active (inactive) phase, both the on-shelf and off-shelf flows are denser (lighter). *Whitworth* [2002] suggests that there are two modes of bottom water in the Australian Antarctic Basin, one associated with a stronger Ross Sea source, and the other associated with a stronger Adélie Land source. It is interesting that he finds the demarcation to occur in 1994, which is consistent with the commencement of our active MGP phase in 1993.

[40] A number of factors influence the interannual variability of the water masses being exchanged. The major atmospheric drivers are surface air temperature and northward wind stress. Years of colder air temperatures are associated with the higher sea ice growth rates and higher ocean to atmosphere heat fluxes we see in the years of stronger HSSW production. In contrast, the strength of northward wind stress is not so readily correlated with the years of denser water mass exchanges. The preconditioned ocean state from early in the season is also clearly of importance. In particular, the volume averaged salinity within the Adélie Depression at the onset of winter regulates the impact of the atmospheric variability upon the dense shelf water formation rate. In years where the volume averaged salinity is higher in the summer months, the onset of dense water production comes earlier and lasts longer, culminating in a greater net annual production. Conversely, when the summer salinities are lower, the onset is later, the production season is shorter, and the net production is reduced. The net ocean to atmosphere heat flux is a good indicator of the strength of dense water formation from year to year, since both are representative of the atmospheric and oceanic components of the coupled system.

[41] There are a number of approaches that could be taken in order to improve our estimates of dense water formation associated with the MGP. Clearly the distribution of icebergs and formation of fast ice are important to get the absolute details correct. *Massom et al.* [1998] note that 26 of the 28 East Antarctic polynyas that they consider form in the lee of protruding coastal features, iceberg tongues, or grounded icebergs. The inclusion of a fast ice model [*Heil et al.*, 1996] would be useful in reproducing the observed geometry of the MGP region, but is beyond the scope of the current work. The use of an ice class model, including frazil ice where our model currently has only open water, would be appropriate for better representing the heat exchange and ice growth rate within the polynya. Such a model is currently under development for use with MPIOM (Jari Haapala, personal communication, 2003). Also of importance is the inclusion of ice shelf and ocean interaction to capture the injection of ISW into the Adélie Depression [*Williams and Bindoff*, 2003]. The coupling of ice shelves into z-coordinate ocean models is inappropriate because of the time evolving thickness of the sub-shelf cavities. The development of parameterizations incorporating the lateral fluxes of heat and freshwater at the ice shelf/ocean interface may be a fruitful approach for further work [*Beckmann and Goosse*, 2003]. A more successful approach to coupled ocean and ice shelf modeling has been achieved using bathymetry following s-coordinate models [*Timmermann et al.*, 2002]. Finally, the bipolar stretched grid approach used here is easily adaptable to studies of other regions. Work has commenced on a model giving high resolution over the Terra Nova Bay polynya in the Ross Sea.

[42] **Acknowledgments.** The original HOPE model code was written by Ernst Maier-Reimer at the Max-Planck-Institut for Meteorology. We are grateful to Uwe Mikolajevicz, Johann Jungclaus, Helmuth Haak, and coworkers at the Max Planck Institute for Meteorology for development of the model code; to Matthew Paget for the buoy track comparison; to Rob Massom for satellite imagery; to Angus Munro for postprocessing of model output; and to John Church, Steve Rintoul, and three anonymous reviewers for comments and criticisms that improved the manuscript. Simon Marsland is grateful for travel support from the Antarctic CRC. This work was funded by CSIRO Complex Systems Science.

References

Ainley, D., and S. S. Jacobs (1981), Sea bird affinities for ocean and ice boundaries in the Antarctic, *Deep Sea Res.*, *28*, 1173–1185.

Arakawa, A., and V. R. Lamb (1977), Computational design of the basic dynamical processes of the UCLA General Circulation Model, *Methods Comput. Phys.*, *17*, 173–265.

Beaman, J. R., and P. T. Harris (2003), Seafloor morphology and acoustic facies of the George V Land shelf, *Deep Sea Res., Part II*, *50*, 1343–1355.

Beckmann, A., and H. Goosse (2003), A parameterization of ice shelf-ocean interaction for climate models, *Ocean Modell.*, *5*, 157–170.

Berliand, M. E., and T. G. Berliand (1952), Determining the net long-wave radiation of the Earth with consideration of the effects of cloudiness, *Isv. Akad. Nauk. SSSR Ser. Geofis.*, *1*, 64–78.

Bindoff, N. L., M. A. Rosenberg, and M. J. Warner (2000), On the circulation and water masses over the Antarctic continental slope and rise between 80 and 150°E, *Deep Sea Res., Part II*, *47*, 2299–2326.

Bindoff, N. L., G. D. Williams, and I. Allison (2001), Sea-ice growth and water-mass modification in the Mertz Glacier polynya, East Antarctica, during winter, *Ann. Glaciol.*, *33*, 399–406.

Brennecke, W. E. (1913a), Oceanography of the German Antarctic Expedition: 2, *Ann. Hydrogr. Mar. Meteorol.*, *2–3*, 464–471.

Brennecke, W. E. (1913b), Oceanography of the German Antarctic Expedition: 3, *Ann. Hydrogr. Mar. Meteorol.*, *2–3*, 642–647.

British Oceanographic Data Centre (1994), GEBCO, General Bathymetric Chart of the Oceans, Prenton, England.

Buck, A. L. (1981), New equations for computing vapor pressure and enhancement factor, *J. Appl. Meteorol.*, *20*, 1527–1532.

Budyko, M. I. (1974), *Climate and Life*, edited by D. H. Miller, Academic, San Diego, Calif.

Carmack, E. C. (1977), Water characteristics of the Southern Ocean south of the Polar Front, in *Voyage of Discovery: George Deacon 70th Anniversary Volume*, edited by M. Angel, pp. 15–41, Pergamon, New York.

Comiso, J. C., and A. L. Gordon (1998), Interannual variability in summer sea ice minimum, coastal polynyas and bottom water formation in the Weddell Sea, in *Antarctic Sea Ice: Physical Processes, Interactions, and Variability*, *Antarct. Res. Ser.*, vol. 74, edited by M. O. Jeffries, pp. 293–315, AGU, Washington, D. C.

Deacon, G. E. R. (1937), The hydrology of the Southern Ocean, *Discovery Rep.*, *15*, 3–122.

Fukamachi, Y., et al. (2000), Seasonal variability of bottom water properties off Adélie Land, Antarctica, *J. Geophys. Res.*, *105*(C3), 6531–6540.

Gibson, J. K., P. Kållberg, S. Uppala, A. Hernandez, A. Nomura, and E. Serrano (1997), ERA description, *ECMWF Re-anal. Proj. Rep. Ser. 1*, Eur. Cent. for Medium-Range Weather Forecasts, Reading, England.

Gill, A. E. (1973), Circulation and bottom water production in the Weddell Sea, *Deep Sea Res.*, *20*, 111–140.

Gordon, A. L., and P. Tchernia (1972), Waters of the continental margin off Adélie coast, Antarctica, in *Antarctic Oceanology II: The Australian-New Zealand Sector*, *Antarct. Res. Ser.*, vol. 19, edited by D. E. Hayes, pp. 59–69, AGU, Washington, D. C.

Griffies, S. M., C. Böning, F. O. Bryan, E. P. Chassignet, R. Gerdes, H. Hasumi, A. Hirst, A.-M. Treguir, and D. Webb (2000), Developments in ocean climate modelling, *Ocean Modell.*, *2*, 123–192.

Haak, H., J. Jungclaus, U. Mikolajewicz, and M. Latif (2003), Formation and propagation of great salinity anomalies, *Geophys. Res. Lett.*, *30*(9), 1473, doi:10.1029/2003GL017065.

Heil, P., I. Allison, and V. I. Lytle (1996), Seasonal and interannual variations of the oceanic heat flux under a landfast Antarctic sea ice cover, *J. Geophys. Res.*, *101*, 25,741–25,752.

Hibler, W. D. (1979), A dynamic thermodynamic sea ice model, *J. Phys. Oceanogr.*, *9*, 815–846.

Jacobs, S. S. (1991), On the nature and significance of the Antarctic Slope Front, *Mar. Chem.*, *35*(104), 9–24.

Kalnay, E., et al. (1996), The NCEP/NCAR 40 year-reanalysis project, *Bull. Am. Meteorol. Soc.*, *77*, 437–470.

Kanamitsu, M., W. Ebisuzaki, J. Woollen, S.-K. Yang, J. J. Hnilo, M. Fiorino, and G. L. Potter (2002), NCEP-DOE AMIP-II reanalysis (R-2), *Bull. Am. Meteorol. Soc.*, *83*, 1631–1643.

Kurtz, D. D., and D. H. Bromwich (1985), A recurring, atmospherically forced polynya in Terra Nova Bay, *Antarct. Res. Ser.*, *43*, 177–201.

Large, W. G., and S. Pond (1982), Sensible and latent heat flux measurements over the ocean, *J. Phys. Oceanogr.*, *12*, 464–482.

Levitus, S., T. P. Boyer, M. E. Conkright, T. O'Brien, J. Antonov, C. Stephens, L. Stathoplos, D. Johnson, and R. Gelfeld (1998), *World Ocean Database 1998*, vol. 1, *Introduction, NOAA Atlas NESDIS 18*, 346 pp., Natl. Oceanic and Atmos. Admin., Silver Spring, Md.

Lytle, V. I., A. P. Worby, R. A. Massom, M. Paget, I. Allison, X. Wu, and A. Roberts (2001), Ice formation in the Mertz Glacier polynya, East Antarctica, during winter, *Ann. Glaciol.*, *33*, 368–372.

Marsland, S. J., and J.-O. Wolff (2001), On the sensitivity of Southern Ocean sea ice to the surface freshwater flux: A model study, *J. Geophys. Res.*, *106*, 2723–2741.

Marsland, S. J., H. Haak, J. H. Jungclaus, M. Latif, and F. Röske (2003), The Max-Planck-Institute global ocean/sea ice model with orthogonal curvilinear coordinates, *Ocean Modell.*, *5*, 91–127.

Massom, R. A., P. T. Harris, K. J. Micheal, and M. J. Potter (1998), The distribution and formative processes of latent-heat polynyas in East Antarctica, *Ann. Glaciol.*, *27*, 420–426.

Massom, R. A., K. L. Hill, V. I. Lytle, A. P. Worby, M. J. Paget, and I. Allison (2001), Effects of regional fast-ice and iceberg distributions on the behaviour of the Mertz Glacier polynya, East Antarctica, *Ann. Glaciol.*, *33*, 391–398.

Massom, R. A., K. Jacka, M. J. Pook, C. Fowler, N. Adams, and N. Bindoff (2003), An anomalous late-season change in the regional sea ice regime in the vicinity of the Mertz Glacier Polynya, East Antarctica, *J. Geophys. Res.*, *108*(C7), 3212, doi:10.1029/2002JC001354.

Morales Maqueda, M. A., A. J. Willmott, and N. R. T. Biggs (2004), Polynya dynamics: A review of observations and modeling, *Rev. Geophys.*, *42*, RG1004, doi:10.1029/2002RG000116.

Mosby, H. (1934), The waters of the Atlantic Antarctic Ocean, *Sci. Results Norw. Antarct. Exped. 1927–28*, *11*, 1–131.

Orsi, A. H., G. C. Johnston, and J. B. Bullister (1999), Circulation, mixing and production of Antarctic Bottom Water, *Prog. Oceanogr.*, *43*, 55–109.

Orsi, A. H., W. M. Smethie, and J. B. Bullister (2002), On the total input of Antarctic waters to the deep ocean: A preliminary estimate from chlorofluorocarbon measurements, *J. Geophys. Res.*, *107*(C8), 3122, doi:10.1029/2001JC000976.

Porter-Smith, R. (2003), Bathymetry of the George Vth Land shelf and slope, *Deep Sea Res., Part II*, *50*, 1337–1341.

Rintoul, S. (1998), On the origin and influence of Adélie Land Bottom Water, in *Ocean, Ice, and Atmosphere: Interactions at the Antarctic Continental Margin*, *Antarct. Res. Ser.*, vol. 75, edited by S. S. Jacobs and R. F. Weiss, pp. 151–172, AGU, Washington, D. C.

Roberts, A., I. Allison, and V. I. Lytle (2001), Sensible- and latent-heat-flux estimates over the Mertz Glacier polynya, East Antarctica, from in-flight measurements, *Ann. Glaciol.*, *33*, 377–384.

Rodman, M., and A. L. Gordon (1982), Southern Ocean bottom water of the Australian-New Zealand sector, *J. Geophys. Res.*, *87*, 5771–5778.

Röske, F. (2001), An atlas of surface fluxes based on the ECMWF Re-Analysis—A climatological dataset to force global ocean general circulation models, *Rep. 323*, Max-Planck-Inst. für Meteorol., Hamburg, Germany.

Schodlok, M. P., C. B. Rodehacke, H. H. Hellmer, and A. Beckmann (2001), On the origin of the deep CFC maximum in the eastern Weddell Sea: Numerical model results, *Geophys. Res. Lett.*, *28*, 2859–2862.

Semtner, A. J. (1976), A model for the thermodynamic growth of sea ice in numerical investigations of climate, *J. Phys. Oceanogr.*, *6*, 379–389.

Simmons, A. J., and J. K. Gibson (Eds.) (2000), *ERA-40 Project plan, ERA-20 Project Rep. 1*, 62 pp., Eur. Cent. for Medium-Range Weather Forecasts, Reading, England.

Stommel, H. (1958), The abyssal circulation, *Deep Sea Res.*, *5*, 80–82.

Stommel, H., and A. B. Arons (1960a), On the abyssal circulation of the world ocean: I. Stationary planetary flow patterns on a sphere, *Deep Sea Res.*, *6*, 140–154.

Stommel, H., and A. B. Arons (1960b), On the abyssal circulation of the world ocean: II. An idealised model of the circulation pattern and amplitude in oceanic basins, *Deep Sea Res.*, *6*, 217–233.

Stössel, A. (1992), The Hamburg Sea-Ice Model, *Tech. Rep. 3*, 61 pp., German Clim. Comput. Cent. (DKRZ), Hamburg, Germany.

Stössel, A. (1996), On the ocean's upper boundary conditions in regions influenced by sea ice, *Physica D*, *98*, 614–624.

Stössel, A., and T. Markus (2004), Using satellite-derived ice concentration to represent Antarctic coastal polynyas in ocean climate models, *J. Geophys. Res.*, *109*, C02014, doi:10.1029/2003JC001779.

Timmermann, R., A. Beckmann, and H. H. Hellmer (2001), The role of sea ice in the fresh water budget of the Weddell Sea, *Ann. Glaciol.*, *33*, 419–424.

Timmermann, R., H. H. Hellmer, and A. Beckmann (2002), Simulations of ice-ocean dynamics in the Weddell Sea: 2. Interannual variability 1985–1993, *J. Geophys. Res.*, *107*(C3), 3025, doi:10.1029/2000JC000742.

Wendler, G., C. Stearns, G. Weidner, G. Dargaud, and T. Parish (1997), On the extraordinary katabatic winds of Adélie Land, *J. Geophys. Res.*, *102*, 4463–4474.

Whitworth, T., III (2002), Two modes of bottom water in the Australian-Antarctic Basin, *Geophys. Res. Lett.*, *29*(5), 1073, doi:10.1029/2001GL014282.

Whitworth, T., III, A. H. Orsi, S.-J. Kim. W. D. Nowlin Jr., and R. A. Locarnini (1998), Water masses and mixing near the Antarctic Slope Front, in *Ocean, Ice, and Atmosphere: Interactions at the Antarctic Continental Margin*, *Antarct. Res. Ser.*, vol. 75, edited by S. S. Jacobs and R. F. Weiss, pp. 1–27, AGU, Washington, D. C.

Williams, G. D., and N. L. Bindoff (2003), Wintertime oceanography of the Adélie Depression, *Deep Sea Res., Part II*, *50*, 1373–1392.

Wolff, J.-O., E. Maier-Reimer, and S. Legutke (1997), The Hamburg Ocean Primitive Equation Model HOPE, *Tech. Rep. 13*, 98 pp., German Clim. Comput. Cent. (DKRZ), Hamburg, Germany.

Worthington, L. V. (1981), The water masses of the world ocean: Some results of a fine-scale census, in *Evolution of Physical Oceanography: Scientific Surveys in Honor of Henry Stommel*, edited by B. A. Warren and C. Wunsch, pp. 42–69, MIT Press, Cambridge, Mass.

Wu, X., W. F. Budd, and I. Allison (2003), Modelling the impacts of persistent Antarctic polynyas with an atmosphere-sea-ice general circulation model, *Deep Sea Res., Part II*, *50*, 1357–1372.

Zwally, H. J., J. C. Comiso, and A. L. Gordon (1985), Antarctic offshore leads and polynyas and oceanographic effects, in *Oceanology of the Antarctic Continental Shelf*, *Antarct. Res. Ser.*, vol. 43, edited by S. S. Jacobs, pp. 203–226, AGU, Washington, D. C.

N. L. Bindoff, W. F. Budd, and G. D. Williams, Antarctic Climate and Ecosystems Cooperative Research Centre, GPO Box 252-80, Hobart, Tasmania, 7001, Australia. (n.bindoff@utas.edu.au; w.f.budd@utas.edu.au; gdwillia@postoffice.antcrc.utas.edu.au)

S. J. Marsland, CSIRO Marine Research, GPO Box 1538, Hobart, Tasmania, 7001, Australia. (simon.marsland@csiro.au)